

60 GHz Channel Measurements and Ray Tracing Modeling in an Indoor Environment

Andong Zhou¹, Jie Huang¹, Jian Sun^{1,2}, Qiuming Zhu^{3,4}, Cheng-Xiang Wang⁵, and Yang Yang⁶

¹Shandong Provincial Key Lab of Wireless Communication Technologies, Shandong University, Jinan, 250100, China.

²State Key Lab. of Millimeter Waves, Southeast University, Nanjing, 210096, P.R.China.

³Jiangsu Key Laboratory of Internet of Things and Control Technologies (Nanjing University of Aeronautics and Astronautics).

⁴College of Electronic and Information Engineering Nanjing University of Aeronautics and Astronautics Nanjing, China.

⁵Institute of Sensors, Signals and Systems, School of Engineering & Physical Sciences, Heriot-Watt University, Edinburgh, EH14 4AS, UK.

⁶Shanghai Research Center for Wireless Communications (WiCO), Shanghai, 201210, China.

Email: zhouad_work@163.com, hj_1204@sina.cn, sunjian@sdu.edu.cn, zhuqiuming@nuaa.edu.cn, cheng-xiang.wang@hw.ac.uk, yang.yang@wico.sh

Abstract—Millimeter wave (mmWave) communication has become a promising key technology of the fifth generation (5G) communication systems, and gained extensive interests. In this paper, we examine 60 GHz mmWave channels in an indoor office environment by means of ray tracing method. Based on geometrical optic (GO) and uniform theory of diffraction (UTD), ray tracing method uses computer simulation to approximate the radio wave propagation. The accuracy of ray tracing based simulation is guaranteed by a very detailed three-dimensional (3-D) environment model and proper material electromagnetic parameters. The simulation results including power delay profile (PDP) and normalized power angular spectrum (PAS) are compared with the channel measurement data which is processed by the space-alternating generalized expectation-maximization (SAGE) estimation algorithm. Good agreements between simulated and measured properties of dominant paths are achieved in both line-of-sight (LOS) and non-line-of-sight (NLOS) scenarios. The comparison results indicate that ray tracing can be a useful and reliable method for characterizing 60 GHz channel properties.

Index Terms—60 GHz, mmWave, channel measurements, ray tracing, SAGE.

I. INTRODUCTION

With the increasing use of wireless devices and developments of mobile communications, frequency resource shortage has become a challenging problem. One possible solution is to move frequency up into mmWave bands which can offer wider bandwidth than lower frequency bands to achieve higher data rates. Also, the severe atmospheric attenuation of mmWave bands can allow better frequency reuse. These features make mmWave communication a key technology for 5G wireless communications [1]. Recently, many projects and standardization organizations including MiWebA [2], MiWaveS [3], mmMAGIC [4], METIS [5] and METIS II [6] have worked on channel modeling and sounding at mmWave bands. Since around 60 GHz band there are abundant unlicensed frequency resource, wireless communication at 60 GHz has widely been used to realize high data rate short-range communications.

Extensive channel measurements have been conducted to characterize mmWave wireless communication channels. In [7], measurements of 60 GHz indoor channels based on the

plus sounding technique were conducted. Reasonable ranges of root mean square (RMS) delay spread were given for different scenarios, and small-scale models were also developed using tapped delay line models. Channel measurements in various indoor environments at 60 GHz band were performed using continuous-route and direction-of-arrival measurement campaigns in [8]. Statistical parameters including RMS delay spread, path loss, and shadowing were inspected. The 60 GHz indoor office environment channel measurements were conducted in [9]. The angular characterization was measured through rotated directional antenna (RDA) based method and uniform virtual array (UVA) based method, and a 60 GHz channel model was also provided.

Since channel measurements are not always available due to the device complexity and time consuming, ray tracing methods are proposed for propagation prediction. Simulations based on ray tracing method were widely performed to predict mmWave communication channel parameters, especially the large-scale parameters [12], [13]. Path loss and RMS delay spread were obtained using shooting and bouncing ray (SBR) ray tracing method in [14] and good agreement was achieved with measurements. In [15], measurements and ray tracing simulations were carried out in a conference room, the accuracy of simulated parameters like path loss, RMS delay spread, channel impulse responses and spatial fading characteristics were evaluated.

While large-scale channel properties at 60 GHz band were well studied, investigations about the small-scale properties like delay and angular of multipath components (MPCs) are still lacking. This paper modeled the 60 GHz indoor channel using ray tracing method. High resolution channel properties in delay and angle domains were also compared and verified by channel measurements.

The rest of this paper is organized as follows. Section II describes the indoor office environment and channel measurement procedure. Section III briefly reviews ray tracing method and gives the simulation settings. Simulation and comparison results are presented in Section IV. Conclusions are drawn in Section V.

II. CHANNEL MEASUREMENTS

A. Measurement Environment

The indoor office environment is approximately $7.2 \times 7.2 \times 3$ m³ with two high built windows on the one side while a considerable large window almost cover the other side of wall. Three sides of wall are made of concrete while one is made of plaster board as a partition wall. Floor and ceiling are decorated with anti-static-electricity board. The room is furnished with several desks and chairs, a table and other common office furniture. Desks have a desktop of 0.75 m height with additional 0.45 m clapboards and equipped with graphoscopes and office supplies. These desks are made of frosted surface chipboard while chairs comprise metal and plastic support and fabric cover. Two wooden doors for the office room and a small storage room in the corner of the office room are remained closed during the measurement procedure.

The photo of the office is shown in Fig. 1(a), together with an ichnography Fig. 1(b) consisting of the locations of 12 transmitters (Tx) and the receiver (Rx). There is a metal tripod placed at the Rx position and a trolley carrying the vector network analyzer (VNA) just beside it. Similarly, the antenna positioner supported the Tx antenna with a nearby handcart carrying the signal generator are sat at Tx positions.

B. Measurement System Setup

The measurement system consists of the Keysight E8257D analog signal generator and the Keysight N5227A VNA [9]. Tx to Rx synchronization is guaranteed by two trigger in/out cables and a reference clock cable. The signal generator is used to generate signal which is fed to Tx antenna and fed to the VNA as the reference signal, respectively. The VNA receives the wireless signal through the Rx antenna and the wireline reference signal through the cable.

In UVA based channel measurements, the Tx antenna is supported and shifted by a high precision antenna positioner in a $15 \times 15 \times 15$ hollow cube array with a step of half wavelength. Measured data is processed using the high resolution SAGE algorithm to obtain MPC parameters in angle domain.

The measurement procedure using a 60 GHz center frequency with a bandwidth of 2 GHz results in a time resolution of 0.5 ns. There are 401 sampling frequency points ranging from 59 to 61 GHz. The Tx antenna is an omni-directional antenna with +13 dBm output power, while the Rx antenna is a horn antenna with 25 dBi gain and 10° 3-dB beamwidth. Both Tx and Rx antennas are 1.6 m high.

III. RAY TRACING CHANNEL MODELING

A. Ray Tracing Method

Since channel measurements are hard conducted and time consuming, ray tracing method which calculates reflection and transmission using GO and diffraction by involving UTD is widely used to build an approximate model for wireless communication. Ray tracing method expresses propagation paths by means of rays, which can be reflected and transmitted when interacting with the surface of obstacles and be diffracted

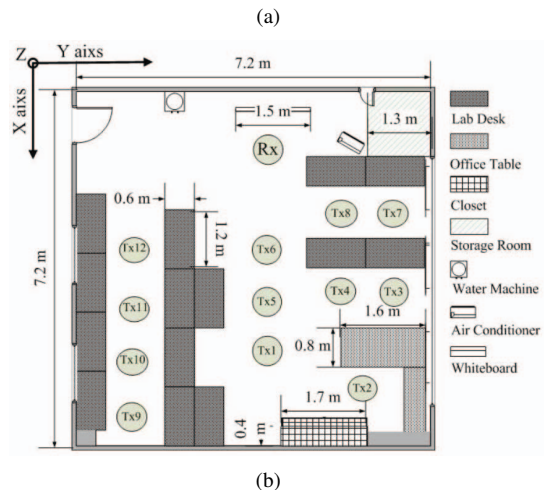


Fig. 1. (a) Photo of the office environment and (b) layout of the office.

when interacting with wedges. According to the interaction of propagation ray, the received power is represented in manner of [16]

$$P_r = \frac{P_t G_t G_r \lambda^2}{(4\pi)^2 d^2} \left[\prod_j R_j \right]^2 \left[\prod_k T_k \right]^2 \left[\prod_l A_l(s', s) D_l \right]^2 \quad (1)$$

where P_t is the transmitted power, G_t and G_r are the antenna gains at Tx and Rx side in the direction of the ray, λ is the wavelength, d is the total length of the ray, R_j is the reflection coefficient of the j -th reflection, T_k is the transmission coefficient of the k -th transmission, D_l is the diffraction coefficient of the l -th diffraction, and $A_l(s', s)$ is the attenuation function. The three coefficients R , T , and D are functions of incident angle and material electromagnetic properties including conductivity and complex permittivity.

The arriving signal at the Rx is formed by MPCs in a wireless communication system, while these MPCs are represented by rays in ray tracing method. The time-invariant channel can be illustrated by the bandlimited channel impulse response (CIR) [16], [17]:

$$h(\tau) = \sum_{n=1}^N A_n \delta(\tau - \tau_n) \exp(-j\psi_n) \quad (2)$$

where $\delta()$ is the Dirac function, A_n , ψ_n , and τ_n denote the amplitude, phase, and delay of the n -th path, respectively.

Although backward ray tracing methods like the traditional image method are simple established and are widely used at lower frequency bands, their complexity are extremely increased when a simulation environment becomes very detailed,

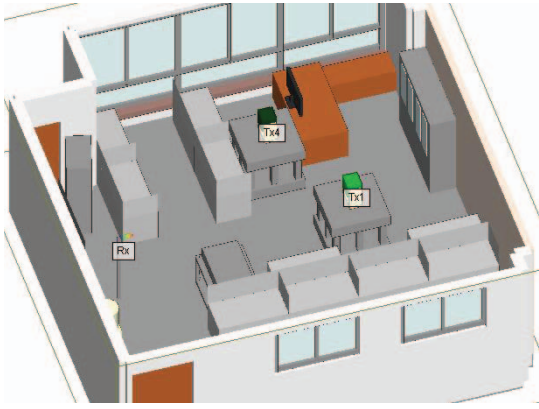


Fig. 2. A 3D ray tracing environment.

i.e., constructed by a large amount of faces. The SBR method can provide higher efficient simulation for complex environments since it demands less in memory and computation time when considering complex environments which contain abundant surfaces.

B. Simulation Setup

A software based on ray tracing, Wireless InSite [18], is used in the investigation. It is based on the SBR method and can offer efficient geometrical calculation. The office environment is modeled using the simulator which is presented in Fig. 2.

Although simplified environment models were widely used for ray tracing at lower frequency bands to achieve higher computational efficiency, highly detailed environment models are indispensable for mmWave simulation. The wavelength at 60 GHz band is much smaller than the dimensions of common office structures and objects, which means these structures and objects are not neglectable. Hence, we setup a detailed described environment model which is precisely built by the simulator.

Office supplies as well as books and computer monitors on the desktops are not modeled because they have irregular shapes which will lead to tremendous increase of computational complexity and are easily shadowed by higher clapboards in the simulation. Similarly, since chairs are about 0.8 m high which is lower than antennas and desks and were positioned nearby the desks, they are neglected in the environment modeling.

The simulator Wireless InSite allows multi-bounces of reflection, transmission, and diffraction. In our work, at most 12 orders of reflection, 3 orders of transmission and 1 order of diffraction are simulated. Scattering caused by surface roughness is not taken into consideration due to the complexity of simulation, while the reflection coefficient is multiplied by a roughness coefficient to express the power loss due to rough surface of objects [19]

$$R = R_s \rho \quad (3)$$

TABLE I
DIELECTRIC PARAMETERS AND ROUGHNESS OF MATERIALS.

Material	Permittivity	Conductivity	Roughness
Drywall	2.48	0.3	0.2
Concrete	6.48	0.166	0.2
Plaster board	2.6	0.001	0.2
Ceiling board	2.58	0.1	0
Glass	6.2	0.1	0
Wood	1.64	0.11	0.1
Chipboard	2.95	0.5	0.5
Metal	1	–	0
Plastic	2.25	0.009	0

where R_s is the reflection coefficient for smooth surface. The roughness coefficient ρ is expressed by

$$\rho = \sqrt{\exp\left(-\frac{8\pi\sigma_h}{\lambda} \sin \theta_i\right)} \quad (4)$$

where θ_i is the incidence angle and σ_h is the standard deviation of the surface variations.

Power threshold of -150 dB and -160 dB are restricted for LOS and NLOS scenarios, respectively. The patterns and positions of Tx and Rx antennas coincide with the measurements.

C. Material Dielectric Parameters

The simulation environment can be represented by the geometrical structures and their electromagnetic properties including conductivity and complex permittivity, where the structures affect the propagation path and the electromagnetic properties affect the received power. These properties of some common building materials were characterized by many high frequency material measurements [20]– [23]. However, the detailed information about the compositions, surfaces, and manufacturing processes of these materials were not detailed in those reviewed papers. Furthermore, temperature and humidity of the material can also influence its electromagnetic properties. Therefore, we slightly adjust the permittivity of some materials in the simulation in order to have a better match with the measurement results. That is, as the materials of structures in our measured office environment are not completely the same as those been tested in references, we adjust their permittivity according to the reference values to get better agreement with our measurements. The used electrical properties of involved materials are summarized in Table I. The units of permittivity and conductivity are F/m and S/m, respectively, while the surface roughness σ_h is given in mm.

IV. RESULTS AND ANALYSIS

In simulations, all twelve Tx locations including both LOS and NLOS scenarios are simulated using ray tracing method. Positions of Tx1, 2, 5, 6, 9, and 10 are classified as LOS scenarios since there is a dominated LOS path in the MPCs. Despite there could probably be a LOS path, we sort positions Tx3, 4, 7, 8, 11, and 12 into NLOS scenarios because they sat outside the main lobe of Rx horn antenna. The Tx1 and Tx4 positions are selected as the typical cases for LOS and

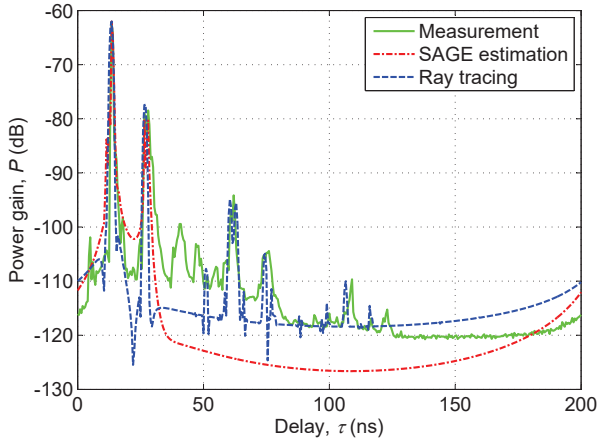


Fig. 3. Comparison of measured, SAGE estimated, and ray tracing based simulated PDPs at Tx1.

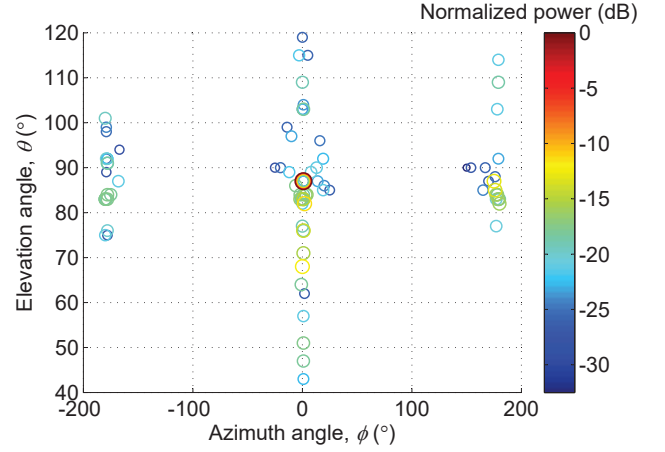
NLOS scenarios, respectively. Simulation results at these two positions are presented in this section for comparison.

A. LOS Scenario: Tx1

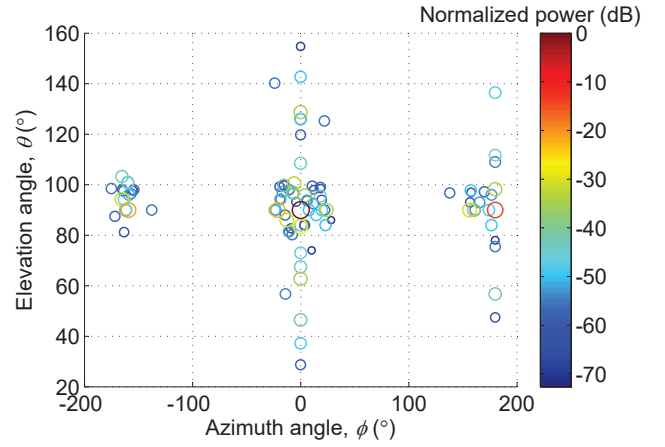
Tx1 is located in (5, 3.6, 1.6) according to the coordinates shown in Fig. 1(b), while Rx is located in (1, 3.6, 1.6). The distance between Tx1 and Rx position is 4 m, and the maximum gain direction of the Rx horn antenna is exactly pointed to the Tx.

The PDPs of measurement, SAGE estimation, and simulation based on ray tracing method are compared in Fig. 3. Here, the simulated PDP is generated from the bandlimited CIR. However, the practical measurement system demands a limited bandwidth, while the bandwidth is not restricted in ray tracing simulation. Therefore we process the simulation data using a 2 GHz bandpass Kaiser window to give it a limited bandwidth for fair comparison. As one of the advantages of ray tracing, the trajectory of paths are intuitively presented in simulations. The LOS path has a small delay of 13.5 ns and large power of approximately -62 dB which is verified by the 4 m separation between Tx and Rx. The second strong peak corresponds to a first-order reflected path which is received by Rx along the direction of maximum gain. These paths with strong power and small delay dominate the propagation in LOS scenario, thus other MPCs with relatively lower power become less important.

It can be seen that the most of the dominant paths are successfully predict, and the PDPs obtained through measurement, estimation, and simulation have achieved a good agreement. However, we can still observe discrepancy between measurement and simulation results. There are several causes for these gaps. One thing that should be noticed is that diffuse scattering is not take into consideration, which might have a considerable contribution in mmWave bands. Also, despite we have tried to use proper dielectric parameters of materials, the distinction between the actual values and the values we use in the simulations may still exist, which may give rise to the power gaps. Another possible reason might be the fact that the



(a)



(b)

Fig. 4. Comparison of PAS at Tx1: (a) UVA estimation and (b) simulation.

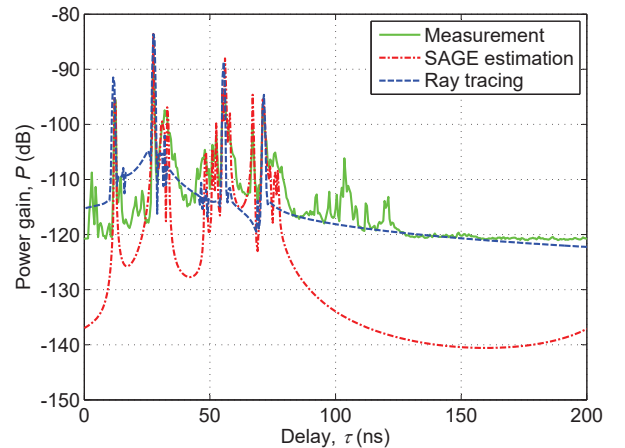


Fig. 5. Comparison of measured, SAGE estimated, and ray tracing based simulated PDPs at Tx4.

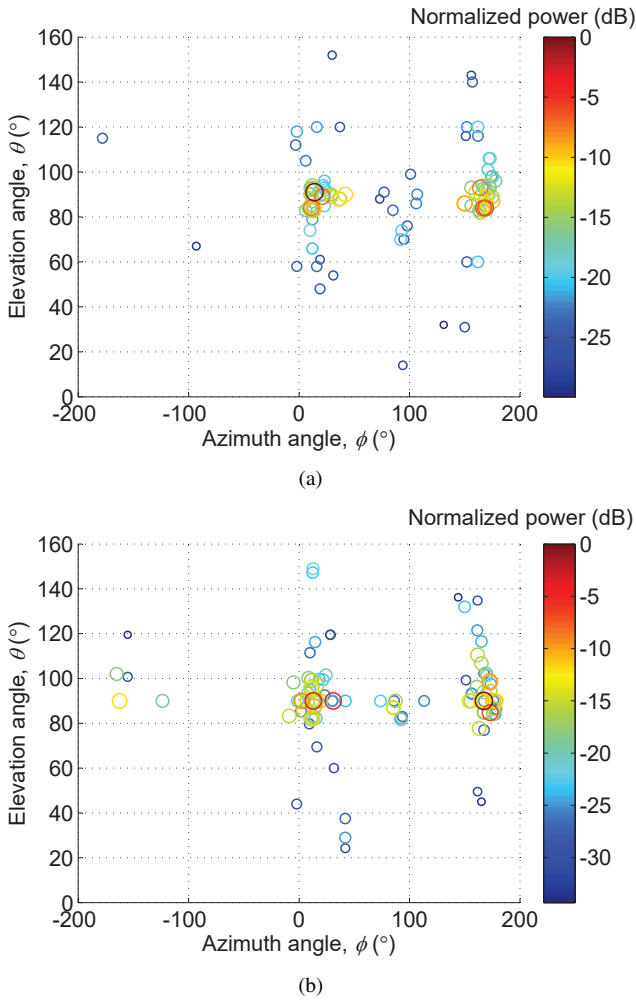


Fig. 6. Comparison of PAS at Tx4: (a) UVA estimation and (b) simulation.

environment model used for simulations can not perfectly fit the actual environment.

Fig. 4 shows the PAS of angle of departures obtained from the SAGE estimation and ray tracing where each colored circle represent a MPC. The estimation uses 100 as the paths number to appropriately capture the energy of received signal. In simulation result, 100 paths with largest received power are selected to make comparison. It can be observed from the results that the normalized power of estimated paths tend to be more intensive while much of simulated MPCs have a much lower power compared to the largest LOS path. Although there are some differences in the power distribution, angles distribution of both are similar for both UVA estimation and ray tracing.

B. NLOS Scenario: Tx4

Position Tx4 is placed at (4, 5.4, 1.6) near one side of the room with a Tx–Rx separation of 3.5 m. Although there is no obstacles between Tx and Rx, the receiving angle of LOS path outrange the beamwidth of Rx antenna.

Fig. 5 shows that the dominant peaks of PDP are well predicted by ray tracing, which indicates that ray tracing can

be reliable in predicting predominant components in radio propagation. The first strong path is the LOS path with a relatively large power and delay of approximately 12 ns, which conform to the Tx and Rx separation of 3.5 m. The other three peaks are dominant multipath components. In our simulation, these paths can be observed reflecting with the front and/or back walls of the room. As these paths have small incident angle when reflect from the walls, they are finally received with relatively larger power. Just like in the LOS scenario, the simulated PDP in the NLOS scenario follows the trend of measured one, although the simulation failed to predict some peaks at the delay around 100 ns. The causes for the differences are identical with these in the LOS case.

The PAS at Tx4 obtained from UVA estimation and ray tracing match better than that at Tx1, as shown in Fig. 6. It can be seen that the MPCs obtained through estimation and simulation distribute similarly. The several red circles with relatively bigger size, which represent the dominant paths, can be observed at an elevation angle of about 90° and azimuth angles of about 15° and 165° .

V. CONCLUSION

In this paper, the 60 GHz wireless communication channel in an indoor office environment has been modeled by ray tracing method. The simulation environment has been carefully modeled to ensure the accuracy. Small-scale channel properties in delay and angle domains have been investigated through simulation. The simulation results have been compared with UVA based channel measurements performed under the same office environment. The peak values of measured and simulated PDPs in both LOS and NLOS scenarios have shown good agreements while some gaps could be observed. In NLOS scenario, PAS of angle of departures for ray tracing and SAGE estimation matches well. Although the power of MPCs tend to have more distinction compared with estimation, the angle distributions are similar in LOS scenario. The comparison results have indicated that ray tracing method is capable for modeling the dominant components of small-scale properties for 60 GHz wireless channel.

ACKNOWLEDGMENT

The authors would like to acknowledge the support from the National Natural Science Foundation of China (Grant No. 61771293, 61371110), Key R&D Program of Shandong Province (Grant No. 2016GGX101014), EU H2020 RISE TESTBED project (Grant No. 734325), EU FP7 QUICK project (Grant No. PIRSES-GA-2013-612652), and EPSRC TOUCAN project (Grant No. EP/L020009/1).

REFERENCES

- [1] T. S. Rappaport, S. Sun, R. Mayzus, H. Zhao, Y. Azar, K. Wang, G. N. Wong, J. K. Schulz, M. Samimi, and F. Gutierrez, "Millimeter wave mobile communications for 5G cellular: It will work!" *IEEE Access*, vol. 1, pp. 335–349, May 2013.
- [2] MiWeba Website, [Online]. Available: <http://www.miweba.eu/>
- [3] MiWaveS Website, [Online]. Available: <http://www.miwaves.eu/>

- [4] mmMAGIC Website, [Online]. Available: <https://5g-mmmagic.eu/>
- [5] METIS Website, [Online]. Available: <https://www.metis2020.com/>
- [6] METIS II Website, [Online]. Available: <https://metis-ii.5g-ppp.eu/>
- [7] N. Moraitis and P. Constantinou, "Measurements and characterization of wideband indoor radio channel at 60 GHz," *IEEE Trans. Wireless Commun.*, vol. 5, no. 4, pp. 880–889, Apr. 2006.
- [8] S. Geng, J. Kivinen, X. Zhao, and P. Vainikainen, "Millimeter-wave propagation channel characterization for short-range wireless communications," *IEEE Trans. Veh. Technol.*, vol. 58, no. 1, pp. 3–13, Jan. 2009.
- [9] X. Wu, C.-X. Wang, J. Sun, J. Huang, R. Feng, Y. Yang, and X. Ge, "60-GHz millimeter-wave channel measurements and modeling for indoor office environments," *IEEE Trans. Antennas Propag.*, vol. 65, no. 4, pp. 1912–1924, Apr. 2017.
- [10] J. Huang, C.-X. Wang, R. Feng, J. Sun, W. Zhang, and Y. Yang, "Multi-frequency mmWave massive MIMO channel measurements and characterization for 5G wireless communication systems," *IEEE J. Sel. Areas Commun.*, vol. 35, no. 7, pp. 1591–1605, July 2017.
- [11] R. Feng, J. Huang, J. Sun, and C.-X. Wang, "A novel 3D frequency domain SAGE algorithm with applications to parameter estimation in mmWave massive MIMO indoor channels," *Sci. China Inf. Sci.*, vol. 60, no. 8, doi: 10.1007/s11432-017-9139-4, Aug. 2017.
- [12] Y. Chang, S. Baek, S. Hur, Y. Mok, and Y. Lee, "A novel two-slope mmWave channel model based on 3D ray-tracing in urban environments," in *Proc. IEEE PIMRC'14*, Washington D.C., Sept. 2014, pp. 222–226.
- [13] J. Pascual-Garcia, M.-T. Martinez-Ingles, J. M. Molina Garcia-Pardo, J. V. Rodriguez, and L. JuanLlacer, "Using tuned diffuse scattering parameters in ray tracing channel modeling," in *Proc. EuCAP'15*, Lisbon, Portugal, Apr. 2015, pp. 1–4.
- [14] M. J. Kazemi, A. Abdipour, and A. Mohammadi, "Indoor propagation MIMO channel modeling in 60 GHz using SBR based 3D ray tracing technique," in *Proc. MMWaTT'12*, Tehran, Iran, Dec. 2012, pp. 25–28.
- [15] M. Peter, W. Keusgen, and R. Felbecker, "Measurement and ray-tracing simulation of the 60 GHz indoor broadband channel: Model accuracy and parameterization," in *Proc. EuCAP'07*, Edinburgh, UK, Nov. 2007, pp. 1–8.
- [16] G. E. Athanasiadou, A. R. Nix and J. P. McGeehan, "A ray tracing algorithm for microcellular and indoor propagation modelling," in *Proc. IEEE ICAP'95*, Eindhoven, the Netherlands, Apr. 1995, vol. 2, pp. 231–235.
- [17] G. E. Athanasiadou and A. R. Nix, "A novel 3-D indoor ray-tracing propagation model: The path generator and evaluation of narrow-band and wide-band predictions," *IEEE Trans. Veh. Technol.*, vol. 49, no. 4, pp. 1152–1168, July 2000.
- [18] Wireless InSite Propagation Software, [Online]. Available: <https://www.remcom.com/wireless-insite-em-propagation-software>
- [19] N. Omaki, T. Imai, K. Kitao, and Y. Okumura, "Improvement of ray tracing in urban street cell environment of non line-of-site (NLOS) with consideration of building corner and its surface roughness," in *Proc. EuCAP'16*, Davos, Switzerland, Apr. 2016, pp. 1–5.
- [20] International Telecommunication Union Recommendation, ITU-R, P.2040-1, "Effect of building materials and structures on radiowave propagation above about 100 MHz", 2015.
- [21] J. Lu, D. Steinbach, P. Cabrol, P. Pietraski, and R. V. Pragada, "Propagation characterization of an office building in the 60 GHz band," in *Proc. EuCAP'14*, The Hague, The Netherlands, Apr. 2014, pp. 809–813.
- [22] K. A. Korolev and M. N. Afsar, "Complex dielectric permittivity measurements of materials in millimeter waves," in *Proc. IRMMW-THz'05*, Williamsburg, VA, Sept. 2005 pp. 62–63.
- [23] D. Ferreira, I. Cuinas, R. F. S. Caldeirinha, and T. R. Fernandes, "A review on the electromagnetic characterization of building materials at micro- and millimetre wave frequencies," in *Proc. EuCAP'14*, The Hague, The Netherlands, Apr. 2014, pp. 145–149.